P-ISSN 2586-9000
E-ISSN 2586-9027
Homepage : https://tci-thaijo.org/index.php/SciTechAsia
Science & Technology Asia
Vol. 24 No. 4 October - December 2019
Page: [42-57]
Original research article

Heat Transfer of Hydromagnetic Convective Flow along a Semi-circular Enclosure Filled with Nanofluids using a Two-dimensional non-homogeneous Model

Sharmin Akter*

Department of Mathematics, BGIFT Institute of Science & Technology, Gazipur, Dhaka 1702, Bangladesh.

Received 4 April 2019; Received in revised form 16 September 2019
Accepted 16 September 2019; Available online 31 October 2019

ABSTRACT

In this paper, the problem of hydromagnetic convective flow along a semi-circular enclosure filled with nanofluids using a two-dimensional non-homogeneous model have been studied numerically. The circular wall of the enclosure is maintained at constant cold temperature whereas various combinations of the thermal boundary conditions at the bottom heated wall are considered. The enclosure is permeated by an inclined uniform magnetic field and the effects of gravity, Brownian motion and thermophoresis are incorporated into the nanofluid model. In the numerical simulation, here is considered water, kerosene as base fluids and Cobalt, Fe_3O_4 as nanoparticles. The Galerkin weighted residual finite element method has been employed to solve the governing partial differential equations after converting them into a non-dimensional form using a suitable transformation of variables. The effects of various parameters such as Hartmann number and Rayleigh number on isotherms have been displayed graphically for Fe_3O_4-water nanofluid. The heat transfer augmentation for various thermal boundary conditions has been done from the bottom heated wall for Fe_3O_4-water and Cobalt-kerosene nanofluid. The results show that the heat transfer rate can be decreased with the increasing values of the Hartmann number but it can be increased by increasing the Rayleigh number. The obtained numerical results also indicate that the variable thermal boundary conditions have significant effects on the flow and thermal fields. Finally, it is observed that the heat transfer rate is higher for Cobalt-kerosene nanofluid than for Fe_3O_4-water nanofluid.

Keywords: Heat transfer; Nanofluid; Finite element method; Thermophoresis; Brownian motion

***Corresponding author:** sharmin.tumpa92@gmail.com **doi:** 10.14456/scitechasia.2019.26

1. Introduction

Nanotechnology plays a vital role for the development of 21st century modern micro- and nano-devices. Recent advances in nanotechnology have allowed researchers to study the next generation heat transfer nanofluids, which consist of a base fluid containing a suspension of ultra-fine nanometer-sized (usually $1-100nm$) solid particles. Nanoparticles can be metal particles such as Cu, Fe, Ag or Au or metallic oxides or nonmetallic oxide particles such as CuO, Al_2O_3, TiO_2, SiO, etc., and the host fluid can be water, ethylene glycol, engine oils, etc. Nanofluids is the term coined by Choi [1] to describe this new class of nanotechnology-based heat transfer fluid that exhibits thermal properties superior to their host fluids or of conventional particle fluid suspensions. Significant features of nanofluids over base fluids include enhanced thermal conductivity, greater viscosity, and enhanced value of critical heat flux. Of these, the most important is the enhanced thermal conductivity, a phenomenon which was first reported by Masuda et al. [2]. Choi [3] reported the use of nanofluids in a wide variety of industries ranging from transportation, energy production and supply to electronics, textiles and paper production. All of these industries deal with heat transfer in some way or another, and thus have a strong need for improved heat transfer mediums. This could possibly be nanofluids because of some potential benefits over normal fluids, such as the large surface area provided by nanoparticles for heat exchange, reduced pumping power due to enhanced heat transfer, minimal clogging, and innovation of miniaturized systems leading to savings of energy and cost. Buongiorno and Hu [4] suggested the possibility of using nanofluids in advanced nuclear systems. Buongiorno suggested a new model based on the mechanics of nanoparticles/base-fluid relative velocity. He took the absolute velocity of nanoparticles to be the sum total of the base-fluid velocity and a relative velocity, (which he calls a slip velocity). Considering seven slip mechanisms- inertia, Brownian diffusion, thermophoresis, diffusophoresis, Magnus effects, fluid drainage and gravity settling, he concluded that in the absence of turbulent effects, Brownian diffusion and thermophoresis dominate. Based on these two effects, he derived the conservation equations. Comprehensive literature reviews of nanofluids can be found in the books by Das et al. [5], and in the papers by Buongiorno [6], Wong and De Leon [7], Manca et al. [8], Mahian et al. [9] etc.

Convective heat transfer in nanofluid filled enclosures has drawn the attraction of many researchers in recent years. In this context, numerous researchers have studied and reported results on convective heat transfer in nanofluids considering various flow conditions in different enclosures. A few of them are Tiwari and Das [10], Ho et al. [11, 12], Abu-Nada [13], Abu-Nada and Oztop [14], Aminossadati and Ghasemi [15], and Muthtamilselvan et al. [16]. Recently, Sheremet et al**.** **[**17**]** studied three-dimensional natural convection in a porous enclosure filled with a nanofluid using Buongiorno's mathematical model.

As per authors' knowledge, the literature review revealed that non-uniform thermal boundary conditions taken into the two-component Buongiorno's mathematical model in a semi-circular shaped solar thermal collector which is filled with nanofluid has not been studied yet. Thus, keeping in mind the engineering and industrial applications of nanofluids we have investigated the convective heat transfer characteristics of nanofluids inside a semi-circular shaped solar thermal collector which is filled with nanofluid with thermal boundary conditions at the bottom heated wall using the two-component Buongiorno's mathematical model. The study was carried out numerically with an

accurate numerical procedure, and the related results are shown graphically in the form of isotherms whereas the average Nusselt numbers are displayed in tabulated form. The reason for choosing a semi-circular enclosure is that, it has practical application in the field of solar thermal collectors. It is hoped that the challenge of augmentation of heat transfer in solar thermal collectors can be met with this model.

2. Problem Formulation

2.1 Physical and Mathematical Modeling

Here is considered a steady, laminar, incompressible two-dimensional natural convection flow in a semi-circular enclosure of length L filled with nanofluids. Dimensional coordinates with the $x-$axis measuring along the bottom wall and $y-$axis being normal to it. The geometry of 2D view with coordinate systems is schematically shown in Fig. 1. The bottom wall of the enclosure is heated which is maintained at temperature as $T = T_h$ that means uniformly heated temperature. Beside this we have considered two non-uniformly heated temperature as $T = T_c + (T_h - T_c)\frac{x}{L}(1-\frac{x}{L})$ and $T = T_c + (T_h - T_c)(\frac{a}{L})\sin(4Kx)$ for comparing isotherms figures and heat transfer rate among these three cases. The round wall is kept at low temperature as $T = T_c$. Due to the uniformly distributed nanoparticles inside the base fluid, the nanoparticles volume fraction on the entire domain has been taken uniform as $C = C_h$. The amplitude of the wave is a and the wave number is $K = \frac{2\pi}{L}$. In the present study, it has taken water, kerosene as base fluids and Cobalt, Fe_3O_4 as nanoparticles. Gravity, thermophoresis and Brownian diffusion effects are included in this study in the absence of any chemical reaction. The base fluids and the solid nanoparticles are assumed to be in thermal equilibrium. The enclosure is permeated by a uniform magnetic field $\mathbf{B} = B_x\mathbf{i} + B_y\mathbf{j}$ of constant magnitude $B_0 = \sqrt{{B_x}^2 + {B_y}^2}$, where i, j are the unit vectors along the coordinate axis. The direction of the magnetic field makes an angle γ with the positive $x-$axis.

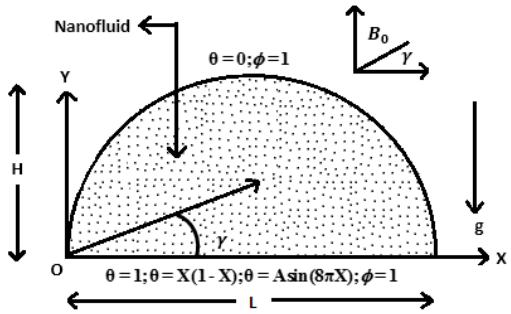

Fig. 1. 2D view of the schematic of the physical model with dimensionless boundary conditions.

A set of governing equations has been formed assuming that the nanofluid is Newtonian and the flow is steady and laminar. The incompressible Navier-Stokes equations have been applied for the two-dimensional flow. The Boussinesq approximation has been applied to consider the density variation. Conservation laws of mass, momentum, energy and nanoparticles volume fraction have been modeled through the accompanying mathematical equations. Within the framework of the above-noted assumptions, the governing equations for this model can be written as:

Continuity equation:

$$\frac{\partial u}{\partial x} + \frac{\partial v}{\partial y} = 0 \qquad (1)$$

Momentum equation in $\mathrm{x}-$direction:

$$\frac{\partial(u^2)}{\partial x}+\frac{\partial(uv)}{\partial y}=\frac{1}{\rho_f}[-\frac{\partial p}{\partial x}+\mu_f\nabla^2 u \quad (2)$$
$$+\sigma_f B_0^2(v\sin\gamma\cos\gamma-u\sin^2\gamma)]$$

Here, μ_f is called dynamic viscosity of fluid particle and it is constant.

Momentum equation in $y-$direction:

$$\frac{\partial(uv)}{\partial x}+\frac{\partial(v^2)}{\partial y}=\frac{1}{\rho_f}[-\frac{\partial p}{\partial y}+\mu_f\nabla^2 v+$$
$$\sigma_f B_0^2(\mathrm{u}\sin\gamma\cos\gamma-v\cos^2\gamma)+(1-\mathrm{C}_C) \quad (3)$$
$$(\mathrm{T}-\mathrm{T}_C)]\rho_f\beta_f g-(C-C_C)(\rho_p-\rho_f)g$$

Energy equation:

$$\frac{\partial(uT)}{\partial x}+\frac{\partial(vT)}{\partial y}=\alpha_f\nabla^2 T+\frac{(\rho C_p)_p}{(\rho C_p)_f}\{D_B$$
$$(\frac{\partial C}{\partial x}\frac{\partial T}{\partial x}+\frac{\partial C}{\partial y}\frac{\partial T}{\partial y})+\frac{D_T}{T_c}[(\frac{\partial T}{\partial x})^2+(\frac{\partial T}{\partial y})^2]$$
(4)

Conservation equation for the nanoparticles:

$$\frac{\partial(uC)}{\partial x}+\frac{\partial(vC)}{\partial y}=D_B\nabla^2 C+\frac{D_T}{T_c}\nabla^2 T \quad (5)$$

where, $\nabla^2=\frac{\partial^2}{\partial x^2}+\frac{\partial^2}{\partial y^2}$ is the Laplace operator and other quantities are defined in the nomenclature.

2.2 Boundary Conditions

The appropriate boundary conditions for the above stated model are as follows:

At the bottom wall:

Case-I:

$$u=v=0, T=T_h, C=C_h \quad (6.a)$$

Case-II:

$$u=v=0,$$
$$T=T_c+(T_h-T_c)\frac{x}{L}(1-\frac{x}{L}), C=C_h \quad (6.b)$$

Case-III:

$$u=v=0,$$
$$T=T_c+(T_h-T_c)(\frac{a}{L})\sin(4Kx), C=C_h \quad (6.c)$$

At the circular wall:

$$u=v=0, T=T_c, C=C_h \quad (6.d)$$

3. Dimensional Analysis

Dimensional analysis is one of the most important mathematical tools in the study of fluid mechanics. It has some advantages. Non-dimensionalization gives freedom to analysis for any system irrespective of its material properties. It also reduces the number and complexity of experimental variables that affect a given physical phenomena. Dimensionless equations provide an insight into the parameters that control the whole system. The results will be independent of the size of the geometry. Before doing an experiment one can get insight into the physical problem. Now we introduce the following non-dimensional variables:

$$\left.\begin{aligned} X=\frac{x}{L}, Y=\frac{y}{L}, \mathrm{A}=\frac{a}{L}, U=\frac{uL}{\alpha_f},\\ V=\frac{vL}{\alpha_f}, P=\frac{(p+\rho_f g_y)L^2}{\rho_f{\alpha_f}^2},\\ \theta=\frac{T-T_C}{T_h-T_C}, \phi=\frac{C-C_C}{C_h-C_C} \end{aligned}\right\} \quad (7)$$

Using (7) into (1) - (5) we obtain the dimensionless equations as follows:

$$\frac{\partial U}{\partial X}+\frac{\partial V}{\partial Y}=0 \quad (8)$$

$$\frac{\partial(U^2)}{\partial X}+\frac{\partial(UV)}{\partial Y}=-\frac{\partial P}{\partial X}+\mathrm{Pr}\nabla^2 U \quad (9)$$
$$+\mathrm{Pr}\,Ha^2(V\sin\gamma\cos\gamma-U\sin^2\gamma)]$$

$$\frac{\partial(UV)}{\partial X}+\frac{\partial(V^2)}{\partial Y}=-\frac{\partial P}{\partial Y}+\Pr\nabla^2 V+Ra\Pr(\theta-\mathrm{Nr}\,\phi)+\Pr \mathrm{Ha}^2(U\sin\gamma\cos\gamma-V\cos^2\gamma) \quad (10)$$

$$\frac{\partial(U\theta)}{\partial X}+\frac{\partial(V\theta)}{\partial Y}=\nabla^2\theta+Nb(\frac{\partial\phi}{\partial X}\frac{\partial\theta}{\partial X}+\frac{\partial\phi}{\partial Y}\frac{\partial\theta}{\partial Y})+Nt[(\frac{\partial\theta}{\partial X})^2+(\frac{\partial\theta}{\partial Y})^2] \quad (11)$$

$$\frac{\partial(\mathrm{U}\phi)}{\partial X}+\frac{\partial(\mathrm{V}\phi)}{\partial Y}=\frac{1}{Le}\nabla^2\phi+\frac{Nt}{LeNb}\nabla^2\theta \quad (12)$$

The non-dimensional parameters which appear in equation (8)-(12) are as follows:

The dimension-less amplitude	$A=\frac{a}{L}=1$
Prandtl number	$\Pr=\frac{\mu_f}{\rho_f\alpha_f}=6.8377$
Hartmann number	$Ha=B_0L\sqrt{\frac{\sigma_f}{\mu_f}}=20$
Rayleigh number	$Ra=\frac{g\beta_f(1-C_c)(T_h-T_c)L^3}{\alpha_f\nu_f}=1\times10^6$
Buoyancy ratio parameter	$Nr=\frac{(\rho_p-\rho_f)(C_h-C_c)}{\rho_f\beta_f(1-C_c)(T_h-T_c)}=0.001$
The thermo-phoresis parameter	$Nt=\frac{(\rho C_p)_p}{(\rho C_p)_f}\frac{D_T(T_h-T_c)}{T_c\alpha_f}=6.9994\times10^7$
Brownian motion parameter	$Nb=\frac{(\rho C_p)_p}{(\rho C_p)_f}\frac{D_B(C_h-C_c)}{\alpha_f}=2.4795\times10^7$
Lewis number	$Le=\frac{\alpha_f}{D_B}=33591$

The non-dimensional boundary conditions become
On the bottom wall:

Case-I:

$$U=V=0,\theta=1,\phi=1 \quad (13.a)$$

Case-II:

$$U=V=0,\theta=X(1-X),\phi=1 \quad (13.b)$$

Case-III:

$$U=V=0,\theta=A\sin(8\pi X),\phi=1 \quad (13.c)$$

On the circular wall:

$$U=V=0,\theta=0,\phi=1 \quad (13.d)$$

4. Evaluation of average Nusselt number

The most important physical quantities for this model are the average Nusselt numbers Nu_{ave} along the heated wall which is calculated from the following expression:

$$Nu_{ave}=-\int_0^1\frac{\partial\theta}{\partial Y}dX \quad (14)$$

5. Thermal & Physical properties of nanofluids

The thermophysical properties of base fluids and nanoparticles are presented in Table 1. (see Oztop and Abu-Nada, [18]), (see Rahman and Al-Hatmi, [19]) and (see Rahman et al. [20]).

Table 1. Thermophysical properties of base fluids and solid nanoparticles.

Physical properties	**Water** (H_2O)	**Kerosene**	Fe_3O_4	**Cobalt**
$C_p(JKg^{-1}K^{-1})$	4179	2090	670	420
$\rho(Kgm^{-3})$	997.1	780	5180	8900
$k(Wm^{-1}K^{-1})$	0.613	0.149	80.4	100
$\mu(Ns/m^2)$	0.001003	0.00164	-	-
$\beta(K^{-1})$	21×10^{-5}	99×10^{-5}	20.6×10^{-5}	1.3×10^{-5}
$\alpha(m^2/s)$	1.47×10^{-7}	9.14×10^{-8}	-	2.67×10^{-5}
Pr	6.8377	23.004	-	
$\sigma[S/m]$	5.5×10^{-6}	6×10^{-10}	1.12×10^{5}	16.02×10^{6}

6. Computational Procedure

The governing dimensionless equations (8)-(12) along with the boundary conditions (13) are solved numerically by employing the Galerkin weighted residual finite element method. The detail of this method is well described by Zienkiewicz and Taylor [21], and Rahman and Uddin [22]. In this method, the solution domain is discretized into finite element meshes, which are composed of non-uniform triangle elements. Six node triangular elements are used in this work for the development of the finite element equations. All six nodes are associated with velocities and temperature as well as isoconcentration; only the corner nodes are associated with pressure. This means that a lower order polynomial is chosen for pressure, which is satisfied through the continuity equation. Then the nonlinear governing partial differential equations (i.e. conservation of mass, momentum and energy equations) are transferred into a system of integral equations by applying the Galerkin weighted residual method. The integration involved in each term of these equations is performed by using Gauss's quadrature method. The nonlinear algebraic equations so obtained are modified by imposition of boundary conditions. To solve the set of the global nonlinear algebraic equations in the form of a matrix, the Newton-Raphson iteration technique has been adapted through partial differential equation solver with fundamental interface. The convergence condition of the numerical solution along with error estimation has been set to $\langle I^{m+1} - I^m \rangle \le 10^{-5}$, where I is the general dependent variable (U,V,θ,ϕ) and m is the number of iteration. In the finite element method, the mesh generation is the technique to divide a domain into a set of sub-domains, called finite element, control volume, etc. The discrete locations are defined by the numerical grid, at which the variables are to be calculated. Meshing the complicated geometry makes the finite element method a powerful technique to solve the boundary value problems occurring in a range of engineering applications. Fig.2 displays mesh configuration of the present physical domain with triangular finite elements.

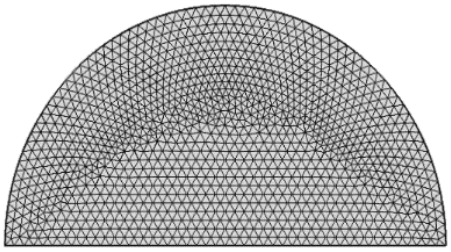

Fig. 2. Mesh structure of the physical domain with triangular finite elements.

For grid sensitivity test, an extensive mesh testing procedure is conducted to guarantee a grid-independent solution for $Ra = 10^4$ and Pr =6.8377 in a semi-circular shaped enclosure. In the present work, we examine five different non-uniform grid systems with the following number of elements within the resolution field: 2350, 3744, 5876, 26906, and 102718. The numerical design was carried out for highly precise key in the average Nusselt number (Nu_{ave}) for the above-mentioned elements to develop an understanding of the grid fine-ness as shown in Table 2. The scale of Nu_{ave} for 26906 elements shows a little difference from the results obtained for the other elements. Hence a grid size of 26906 elements is found to meet the requirements of both the grid independency study and the computational time as we see in Fig. 3. In our simulation, we have taken 26906 elements.

Table 2. Grid sensitivity check for Fe_3O_4-H_2O nanofluid at $Ra = 10^4$ & Pr =6.8377 .

Nodes	Elements	Nu_{ave}
1234	2350	0.86814
1947	3744	0.87192
3031	5876	0.87485
13652	26906	0.88185
51745	102718	0.88192

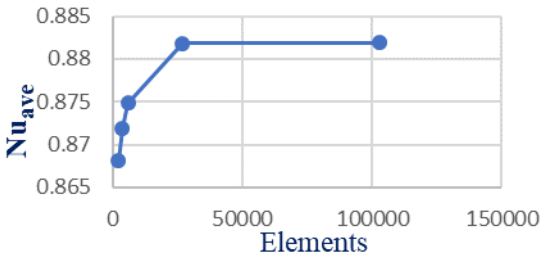

Fig. 3. Average Nusselt number for different elements.

The present numerical code was validated with the published study of Uddin and Rahman [23]. The physical problem studied by Uddin and Rahman [23] was unsteady laminar natural convection inside a semi-circular enclosure. Though the present work is natural convection inside a semi-circular enclosure for steady laminar case, we compare the present work with Uddin and Rahman [23]. Because for the unsteady case, in a sudden time, its behavior is almost steady laminar natural convection without magnetic field. The comparison of the results obtained by the present numerical code with those of Uddin and Rahman [23] with respect to isotherms for different Rayleigh number is shown in Fig.4. The computed results show very good agreement with the Uddin and Rahman [23] solution. This validation boosts the confidence in the numerical outcome of the present study.

10^5	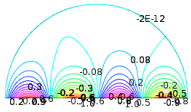	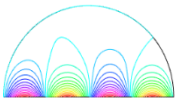
10^6	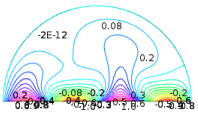	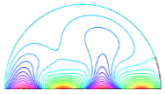
10^7	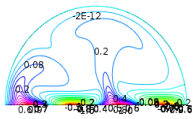	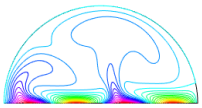
Ra	**Fig. 4.(a)** Uddin and Rahman [23] Isotherms.	**Fig. 4.(b)** Present study Isotherms.

7. Results and Discussion

In this section, a numerical study has been performed through finite element method to analyze the laminar natural convection heat transfer and fluid flow in a semi-circular enclosure filled with nanofluids in the presence of an oriented magnetic field. In the numerical simulation, Fe_3O_4-water and Cobalt-kerosene have been considered. Isotherms are presented graphically for Fe_3O_4-water nanofluid using uniformly heated as well as non-Fe_3O_4-water nanofluid. The default values of the other parameters are considered as $Ha = 20$, $\gamma = 60^0$, $Nr = 0.001$, $Ra = 10^6$ and the dimensionless amplitude of the wave $A = 1$ unless otherwise specified.

uniformly heated temperatures on the bottom wall. The rate of heat transfer at the bottom heated wall for three different cases has been shown in tabular form for Fe_3O_4-water and Cobalt-kerosene nanofluids for a wide range of the controlling parameters. Particular efforts have been focused on the effects of three effective factors such as the Rayleigh number (Ra), the Hartmann number (Ha) and magnetic field inclination angle (γ) on the fluid flow. It is obvious that if the nanoparticles are distributed uniformly in the base fluid, then a greater heat transfer rate is expected. But due to the Brownian motion of the nanoparticles and thermophoretic effects of nanofluids, it is assumed that there is a little bit of concentration difference and it is expected that this concentration difference can be $\Delta C = 0.01$. Thus for Fe_3O_4-water nanofluid with 1% volume fraction nanoparticles of diameter $d_p = 10\text{nm}$, $T_C = 300K$, temperature difference $\Delta T = 10K$, the values of the Brownian diffusion coefficient $D_B = 4.3795 \times 10^{-12}$ and thermal diffusion coefficient $D_T = 3.6841 \times 10^{-12}$ for Fe_3O_4-water nanofluid with these calculated results, the values of $\text{Pr} = 6.8377$, $Nt = 6.9994 \times 10^{-7}$, $Nb = 2.4795 \times 10^{-7}$, $Le = 33591$ have been taken into the numerical simulation for

7.1 Effects of Rayleigh Number (Ra)

The effect of the Rayleigh number $\mathrm{Ra}(\mathrm{Ra}=10^5, \mathrm{Ra}=10^6)$ on the isotherms for uniform and non-uniform cases on the bottom heated wall is shown in Fig. 5(a)-(c) and Fig. 6(a)-(c) for Fe_3O_4-water nanofluid. To identify the efficiency of heat transfer in a fluid, isotherm contours are helpful and also show us about the dictating mode of heat transfer, i.e. whether it is conduction or convection. Fig. 5(a)-(c) and Fig. 6(a)-(c) show isotherm contours for Rayleigh number $Ra=10^5$ and $Ra=10^6$, respectively, with three different thermal boundary conditions. In case-I, the isotherms pattern indicates that at low values of Ra, it shows low convection inside the enclosure, which means the density of isotherms is less at the central of the enclosure. In this case, uniform heating of the bottom wall causes a finite discontinuity in the Dirichlet boundary conditions for the temperature distributions at both edges of the bottom wall. Increasing the value of Ra, convection increases and is formed like a mushroom .In case-II, a non-uniformly heated case, the isotherm contours are seen almost parallel to each other near the heated wall and forming parabolic shape for low values of Ra. This pattern indicates dominance of the conduction mode of heat transfer near the walls at low values of Ra. But, when increasing the value of Ra, the isotherms spread near the centre of the enclosure forming a pattern just like a mushroom. This pattern suggests that heat energy flows into the fluid inside the enclosure from the bottom heated wall. For case-III, a non-uniformly heated bottom wall, there are eight cells formed in almost symmetric manner. Increasing the value of Ra, the isotherms become more distorted due to the stronger convection effects. Here we see that in the mid portion of the cavity, isotherms assume an inverted and irregular shape showing that convection is over riding in that region. This specifies that at higher value of Ra, adding nanoparticles expands convective heat transfer.

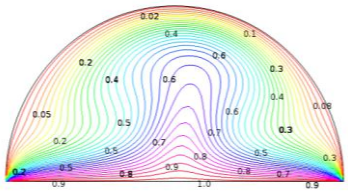

(a) Case - I : θ = 1

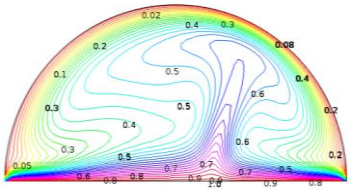

(a) Case - I : θ = 1

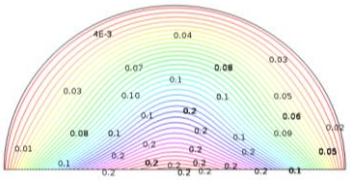

(b) Case - II : θ = X(1 - X)

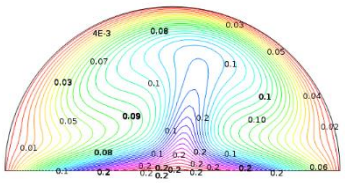

(b) Case - II : θ = X(1 - X)

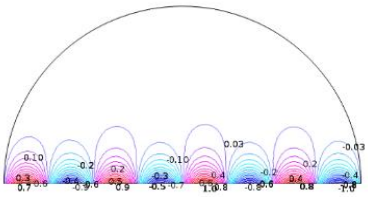

(c) Case - III : θ = Asin(8πX)

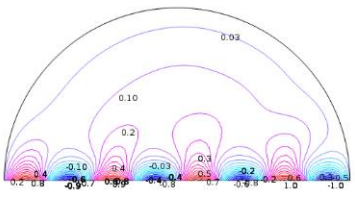

(c) Case - III : θ = Asin(8πX)

Fig. 5.(a)-(c): Isotherms for $Ra = 10^5$ using three different boundary conditions on the bottom heated wall, while $Ha = 20$, $\gamma = 60^0$ & $d_p = 10nm$ are fixed.

Fig. 6.(a)-(c): Isotherms for $Ra = 10^6$ using three different boundary conditions on the bottom heated wall, while $Ha = 20$, $\gamma = 60^0$ & $d_p = 10nm$ are fixed.

7.2 Effects of Hartmann Number (Ha)

The influence of the Hartmann number Ha(Ha = 0, Ha = 50) on the isotherm contours for uniform and non-uniform cases on the bottom heated wall is shown in Fig. 7 (a)-(c) and Fig. 8(a)-(c) for Fe_3O_4-water nanofluid. On the isotherms, from Fig. 7(a)-(c) and Fig. 8(a)-(c), for case-I and case-II, the effect of the Hartmann number (Ha) is more conspicuous which indicates the mode of heat transfer. As it can be observed that for $Ha = 0$, the isotherms pattern is like a plume which means an indication of strong convection. After increasing, when $Ha = 50$, convection is weaker inside the enclosure, which means the isotherms are seen almost parallel to each other near the heated wall and forming a parabolic shape. Thus the Hartmann number acts against convection inside the cavity. For case-III, a non-uniformly heated temperature, there are eight symmetric circular cells on the bottom heated wall and middle cells are extended in the enclosure. However, for all cases when the Lorentz force is considered as Ha increasing, the isotherms start to move away from the bottom heated wall. This means that the temperature gradient inside the cavity decreases as estimated.

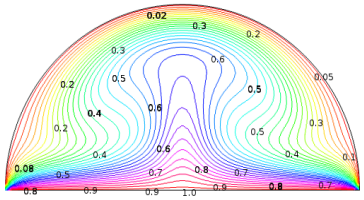

(a) Case - I : θ = 1

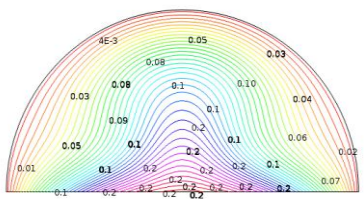

(b) Case - II : θ = X(1 - X)

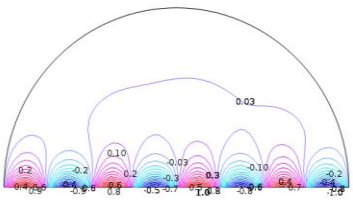

(c) Case - III : θ = Asin(8πX)

Fig. 7.(a)-(c): Isotherms for $Ha = 0$ using three different boundary conditions on the bottom heated wall, while $Ra = 10^5, \gamma = 60^0$ & $d_p = 10nm$ are fixed.

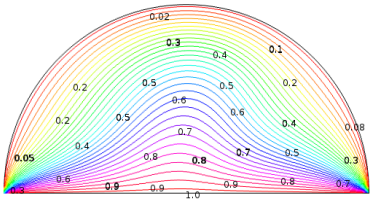

(a) Case - I : θ = 1

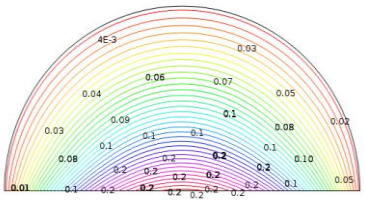

(b) Case - II : θ = X(1 - X)

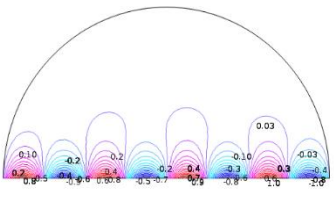

(c) Case - III : θ = Asin(8πX)

Fig. 8.(a)-(c): Isotherms for $Ha = 50$ using three different boundary conditions on the bottom heated wall, while $Ra = 10^5, \gamma = 60^0$ & $d_p = 10nm$ are fixed.

7.3 Effects of the Magnetic Field Inclination Angle*(g)*

The effects of the magnetic field inclination angle (γ) on isotherm contours for uniform and non-uniform cases on the bottom heated wall for Fe_3O_4-water nanofluid are shown in Fig. 9(a)-(c) and Fig. 10(a)-(c). The influence of the direction of the magnetic field on the isotherm contours have been shown in Fig. 9(a)-(c) and Fig. 10(a)-(c) for the three different boundary conditions on the bottom wall of the enclosure. For Case-II, a non-uniform heated condition, we see that the isotherm lines are almost parallel shape for $\gamma = 0^o$ which shows a conduction mode of heat transfer. When the inclination angle changes, both the horizontal and vertical components of the body forces due to the magnetic and buoyancy fields are present and, when $\gamma = 90^o$, this consequently similar parallel pattern can be identified which indicates convective heat transfer. For case-III, there are eight cells which have a similar pattern. However, the temperature field is not affected much by the orientation of the magnetic field like the flow field. The thermal boundary layer becomes slightly thick and the isotherms are more concentrated for a uniformly heated wall than for a non-uniformly heated wall.

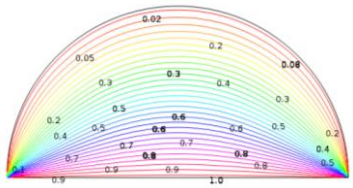

(a) Case - I : θ = 1

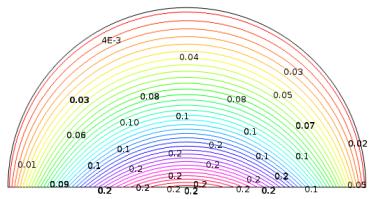

(b) Case - II : θ = X(1 - X)

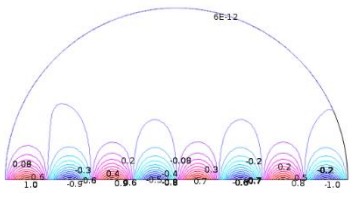

(c) Case - III : θ = Asin(8πX)

Fig. 9.(a)-(c): Isotherms for $\gamma = 0^o$ using three different boundary conditions on the bottom heated wall, while $Ra = 10^5$, $Ha = 100$, $d_p = 10nm$ are fixed.

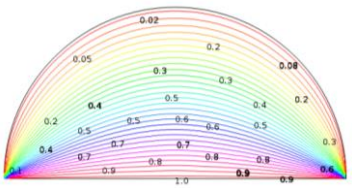

(a) Case - I : θ = 1

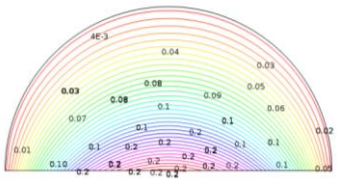

(b) Case - II : θ = X(1 - X)

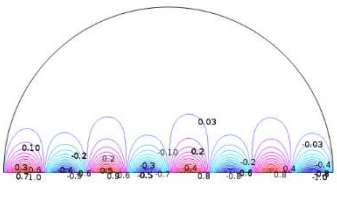

(c) Case - III : θ = Asin(8πX)

Fig. 10.(a)-(c): Isotherms for $\gamma = 90^o$, using three different boundary conditions on the bottom heated wall, while $Ra = 10^5$, $Ha = 100$, $d_p = 10nm$ are fixed.

7.4 Average Nusselt Number

One of the main objectives of this study is to show the effects of the governing parameters, namely the Hartmann number (Ha), magnetic field inclination angle (γ) and Rayleigh number (Ra), on the rate of heat transfer at the heated wall of the enclosure filled with nanofluids.

Here we consider three different types of boundary condition, such as case-I; uniformly heated wall that means $\theta = 1$, case-II; non-uniformly heated wall where $\theta = X(1-X)$, case-III; non-uniformly heated wall where $\theta = Asin(8\pi X)$. Table 3 and Table 4 are displayed to satisfy this goal. From these tables, we observed that in all cases, the rate of heat transfer is decreased with the increasing values of the Hartmann number (Ha), and the magnetic field inclination angle (γ) for Fe_3O_4-water. For Cobalt-kerosene, the rate of heat transfer is also decreased with increasing the Hartmann number (Ha), as well as the inclination angle (γ). As we know, an applied magnetic field on the flow domain creates a Lorentz force which in turn retards the fluid motion. As a consequence, the flow carries less heat from the hot surface to the fluid which results in a decrease of the heat transfer rate of nanofluids. But we also observed that for case-I and case-III, the heat transfer rate of Fe_3O_4-water is greater than Cobalt-kerosene nanofluid. But for case-II, the heat transfer rate of Cobalt-kerosene is greater than Fe_3O_4-water nanofluid.

Table 3. Variation of the average Nusselt number (Nu_{ave}) for Fe_3O_4-water & Cobalt-kerosene nanofluids with different values of Hartmann number *(Ha),* and magnetic field inclination angle (γ) with respect to different boundary conditions.

Ha	$\gamma(^0)$	Thermal boundary conditions	Fe_3O_4-water (Nu_{ave})	Cobalt-kerosene (Nu_{ave})
1	0	Case-I	14.22928	6.74521
		Case-II	0.87852	1.80522
		Case-III	25.72961	22.87174
1	90	Case-I	14.22922	6.7452
		Case-II	0.87852	1.80547
		Case-III	25.73069	22.87175
50	0	Case-I	11.87655	6.69057
		Case-II	0.87423	1.27668
		Case-III	24.47595	22.87175
50	90	Case-I	11.64309	6.68896
		Case-II	0.87384	1.27254
		Case-III	24.7187	22.87129
100	0	Case-I	9.29628	6.68962
		Case-II	0.87392	0.92659
		Case-III	23.43185	22.87101
100	90	Case-I	8.80836	6.68811
		Case-II	0.87356	0.89355
		Case-III	23.70174	22.87104

From table 4, we observe that, for Fe_3O_4-water & Cobalt-kerosene in all cases, the rate of heat transfer is decreased with the increasing values of the Rayleigh number (Ra) while it increases with the increment of Hartmann number (Ha), and for both nanofluids, the heat transfer rate shows little difference.

Table 4. Variation of the average Nusselt number (Nu_{ave}) for Fe_3O_4-water & Cobalt-kerosene nanofluids with different values of Rayleigh number (Ra) and Hartmann number (Ha), while magnetic field inclination angle (γ) is fixed using three different boundary conditions.

Ra	*Ha*	Thermal boundary conditions	Fe_3O_4-water (Nu_{ave})	Cobalt-kerosene (Nu_{ave})
10^4	0	Case-I	6.47404	6.77625
		Case-II	0.87532	0.87531
		Case-III	22.87174	22.87174
10^4	30	Case-I	6.42398	6.69351
		Case-II	0.87417	0.87417
		Case-III	22.87144	22.87141

Ra	*Ha*	Thermal boundary conditions	Fe_3O_4-water (Nu_{ave})	Cobalt-kerosene (Nu_{ave})
10^4	70	Case-I	6.41919	6.68869
		Case-II	0.87384	0.87384
		Case-III	22.87109	22.87107
10^4	150	Case-I	6.41921	6.68837
		Case-II	0.87377	0.87377
		Case-III	22.87091	22.87092
10^5	0	Case-I	9.18887	9.46998
		Case-II	1.03414	1.03414
		Case-III	22.95389	22.95385
10^5	30	Case-I	7.71597	8.04366
		Case-II	0.89068	0.89068
		Case-III	22.92141	22.91791
10^5	70	Case-I	6.5048	6.74984
		Case-II	0.87367	0.87367
		Case-III	22.88935	22.88724
10^5	150	Case-I	6.41558	6.6751
		Case-II	0.87217	0.87217
		Case-III	22.87382	22.87378

7. Conclusions

In the present study, the problem of steady hydromagnetic laminar natural convective flow and heat transfer of nanofluid inside a semi-circular enclosure under the influence of an oriented magnetic field is studied numerically using a two-component thermal equilibrium model. All numerical results are discussed from the physical point of view. From the numerical simulations, the major outcomes are as follows:

I. Better heat transfer through convection is achieved for higher values of the Rayleigh number.

II. Higher values of *Ra* confirm better heat transfer through convection than conduction.

III. The rate of heat transfer is decreased with the increasing values of the Hartmann number *(Ha)*, and the magnetic field inclination angle (γ).

IV. The heat transfer rate is higher for Cobalt-kerosene nanofluid than Fe_3O_4-water nanofluid in case-II, while the heat transfer rate is higher for Fe_3O_4-water nanofluid for case-I and case-III with respect to the Hartmann number and the magnetic field inclination angle.

V. In case-III, we get the highest heat transfer rate for Fe_3O_4-water nanofluid.

VI. The heat transfer rate is higher for Cobalt-kerosene nanofluid than Fe_3O_4-water nanofluid in case-I with respect to Rayleigh number and Hartmann number.

Nomenclature

a	dimensional amplitude of the wave (m)
A	dimensionless amplitude of the wave
B_0	magnetic field strength ($\mathrm{kg}\, s^{-2}A^{-1}$)
C_p	specific heat at constant pressure ($Jkg^{-1}K^{-1}$)
C	nanoparticle volume fraction
D_B	Brownian diffusion coefficient (m^2s^{-1})
D_T	thermophoretic diffusion coefficient (m^2s^{-1})
g	gravitational acceleration (ms^{-1})
H	height of the cavity (m)
Ha	Hartmann number
k	thermal conductivity ($Wm^{-1}K^{-1}$)
K	wave number
L	length of the cavity (m)
Le	Lewis number
Nb	Brownian diffusion parameter
Nr	buoyancy ratio parameter
Nt	thermophoresis parameter
Nu	Nusselt number
p	dimensional pressure (Pa)
P	dimensionless pressure
Pr	Prandtl number
Ra	Rayleigh number
T	temperature (K)
(u,v)	dimensional velocity components (ms^{-1})
(U,V)	dimensionless velocity components
(x,y)	dimensional coordinates (m)
(X,Y)	dimensionless coordinates

Greek symbols

α	thermal diffusivity (m^2s^{-1})
β	coefficient of thermal expansion (K^{-1})
γ	magnetic inclination angle (^{o})
σ	electric conductivity ($Wm^{-1}K^{-1}$)
θ	dimensionless temperature
ϕ	normalized nanoparticle volume fraction
ψ	stream function
μ	dynamic viscosity ($kgm^{-1}s^{-1}$)
ρ	density (kgm^{-3})
(ρC_p)	heat capacity ($JK^{-1}m^{-3}$)

Subscripts

ave	average
c	condition at cold wall
f	base fluid
h	condition at heated wall
p	solid nanoparticle

References

[1] Choi S. (1995): Enhancing thermal conductivity of fluids with nanoparticles. In: Signier DA, Wang HP (eds.) Development and applications of non-Newtonian flows, 231(66); 99–105.

[2] Masuda H., Ebata A., Teramae K., Hishinuma N. (1993): Alteration of thermal conductivity and viscosity of liquid by dispersing ultra-fine particles, Netsu Bussei 7; 227–233.

[3] Choi S. (1999): Nanofluid technology, current status and future research, energy technology division, argonne national laboratory, Argonne.

[4] Buongiorno J., Hu W. (2005): Nanofluid coolants for advanced nuclear power plants, Paper no. 5705, in: Proceedings of ICAPP '05, Seoul, 15-19.

[5] Das S. K., Choi S. U. S., Wenhua Y. and Pradeep T. (2007): Nonofluids, science and technology, John Wiley and Sons.

[6] Buongiorno J. (2006): Convective transport in nanofluids. ASME J. Heat Transfer, 128; 240-250.

[7] Wong K. V. and De Leon O. (2010): Applications of nanofluids, current and future. Adv. Mech. Eng., Art. ID 519659; 11.

[8] Manca O., Jaluria Y., and Poulikakos D. (2010): Heat transfer in nanofluids, Advances in Mech. Eng. Art. ID 380826 (2).

[9] Mahian O., Kianifar A., Kalogirou S. A., Pop I. and Wongwises S. (2013): A review of the applications of nanofluids in solar energy, Int. J. Heat Mass Trans. 57; 582–594.

[10] Tiwari R. K., Das M. K. (2007): Heat transfer augmentation in a two-sided lid-driven differentially heated square cavity utilizing nanofluids. Int. J. Heat Mass Trans., 50; 2002–2018.

[11] Ho C. J., Chen M. W., Li Z. W. (2008): Numerical simulation of natural convection of nanofluid in a square enclosure: effects due to uncertainties of viscosity and thermal conductivity, Int. J. Heat Mass Transf., 51; 4506–4516.

[12] Ho C. J., Chen M. W., Li Z. W. (2007): Effect of natural convection heat transfer of nanofluid in an enclosure due to uncertainties of viscosity and thermal conductivity, In Proceedings of ASME/JSME Thermal Engineering, Summer Heat Transfer Conference HT, 1; 833–841.

[13] Abu-Nada E. (2007): Application of nanofluids for heat transfer enhancement of separated flows encountered in a backward facing step, Int. J. Heat Fluid Flow 29; 242–249.

[14] Abu-Nada E., Oztop H.F. (2009): Effects of inclination angle on natural convection in enclosures filled with Cu-water nanofluid, Int. J. Heat Fluid Flow 30; 669–678.

[15] Aminossadati S. M., Ghasemi B. (2009): Natural convection cooling of a localized heat source at the bottom of a nanofluid-filled enclosure, Eur. J. Mech B/Fluids 28; 630–640.

[16] Muthtamilselvan M., Kandaswamy P., and Lee J. (2010): Heat transfer enhancement of copper-water nanofluids in a lid-driven enclosure, Com. Nonlin. Sci. Numer. Simulat., 15; 1501–1510.

[17] Sheremet M. A., Pop I. and Rahman M. M. (2015): Three-dimensional natural convection in a porous enclosure filled with a nanofluid using Buongiorno's mathematical model. Int. J. Heat Mass trans. 82; 396-405.

[18] Oztop H. F., and Abu-Nada E. (2008): Numerical study of natural convection in partially heated rectangular enclosures filled with nanofluids, Int. J. Heat Fluid Flow, 29; 1326–1336.

[19] Rahman M. M. and Al-Hatmi M. M. (2014): Hydromagnetic boundary layer flow and heat transfer characteristics of a nanofluid over an inclined stretching surface in the presence of convective surface, a comprehensive study, SQU J. Sci. 19(2); 53-76.

[20] Rahman M. M., Rosca A. V.and Pop I. (2014): Boundary layer flow of a nanofluids past a permeable exponentially shrinking/stretching surface with second order slip using Buongiorno's model, Int. J. Heat and Mass Trans., 77; 1133-1143.

[21] Zienkiewicz O. C. and Taylor R. L. (1991): The finite element method, McGraw-Hill; 4.

[22] Uddin M. J., Rahman M. M. (2018): Finite element computational procedure for convective flow of nanofluids in an annulus.

[23] Uddin M. J. and Rahman M. M. (2017): Numerical computation of natural convective heat transport within nanofluids filled semi-circular shaped enclosure using nonhomogeneous dynamic model.